Observation of $2p3d(^1P^o) \rightarrow 1s3d(^1D^e)$ Radiative Transition in He-like Si, S, and Cl Ions

S. Kasthurirangan,[1,2] J. K. Saha,[3] A. N. Agnihotri,[1] S. Bhattacharyya,[4] D. Misra,[1] A. Kumar,[5] P. K. Mukherjee,[6] J. P. Santos,[7] A. M. Costa,[7] P. Indelicato,[8] T. K. Mukherjee,[3] and L. C. Tribedi[1,*]

[1]*Department of Nuclear and Atomic Physics, Tata Institute of Fundamental Research, Colaba, Mumbai 400005, India*
[2]*Department of Physics, Institute of Chemical Technology, Mumbai 400019, India*
[3]*Narula Institute of Technology, Agarpara, Kolkata 700109, India*
[4]*Acharya Prafulla Chandra College, Kolkata 700131, India*
[5]*Nuclear Physics Division, Bhabha Atomic Research Centre, Mumbai 400085, India*
[6]*Ramakrishna Mission Vivekananda University, Howrah 711202, India*
[7]*Centro de Física Atómica, Departamento de Física, Faculdade de Ciências e Tecnologia, FCT, Universidade Nova de Lisboa, P-2829-516 Caparica, Portugal*
[8]*Laboratoire Kastler Brossel, École Normale Supérieure, CNRS, Université P. et M. Curie-Paris 6, Case 74; 4, place Jussieu, 75252 Paris CEDEX 05, France*

(Received 5 September 2013; published 13 December 2013)

We present an experimental determination of the $2p3d(^1P^o) \rightarrow 1s3d(^1D^e)$ x-ray line emitted from He-like Si, S, and Cl projectile ions, excited in collisions with thin carbon foils, using a high-resolution bent-crystal spectrometer. A good agreement between the observation and state-of-the-art relativistic calculations using the multiconfiguration Dirac-Fock formalism including the Breit interaction and QED effects implies the dominance of fluorescent decay over the autoionization process for the $2p3d(^1P^o)$ state of He-like heavy ions. This is the first observation of the fluorescence-active doubly excited states in He-like Si, S, and Cl ions.

DOI: 10.1103/PhysRevLett.111.243201 PACS numbers: 32.30.Rj, 31.15.ac, 31.30.jc, 34.50.Fa

Since the pioneering work of Madden and Codling in 1963 [1], the study of doubly excited states (DES) of helium has been a fundamental topic of research for many decades [1–7]. All these states lie above the first ionization potential of He. Hence, they can be considered to be discrete states embedded in the first ionization continuum [7]. They generally relax via autoionization to the ground state of the He^+ ion. The same is true for the entire isoelectronic sequence of He-like ions where the DES decay via autoionization to the corresponding H-like ions. For some DES, such as $2p^2(^3P^e)$, autoionization is forbidden, and radiative relaxation to a singly excited state may take place. In fact, it is a bound doubly excited state, as $2p^2(^3P^e)$ is the lowest ^3P state of even parity. Simple quantum mechanical considerations lead to the autoionization selection rules [8,9] $\Delta J = 0$, $\Delta\pi = 0$ (i.e., the total angular momentum J and the parity π of the system must be conserved). It may be mentioned that we are considering zero order theory, neglecting the relativistic and other magnetic effects in the above description, i.e., the Russell-Saunders limit for the defined states. The above effects lead to configuration mixing, which is responsible for the competition between autoionization and fluorescence channels.

The DES are of great importance in astrophysics [10] as well as for plasma diagnostics [11,12]. Besides such applications, the fundamental subject of dominance of fluorescence over autoionization decay for some DES has drawn much attention both from theoreticians [13–15] and experimentalists [16–20] in the last decade. All the experimental works are limited to atomic He. Recently, Saha *et al.* [21] have proposed a criterion where it has been shown that the angular part of the wave function is responsible for the dominance of fluorescence over autoionization for some of the DES. It is well known that the angular part of the wave function is independent of atomic number Z; i.e., the angular part is the same for the entire He-like isoelectronic sequence. Hence, if this criterion is true, then one should expect a spectral line corresponding to the $2p3d(^1P^o) \rightarrow 1s3d(^1D^e)$ transition for the He-like ions in an experiment. This is exactly what has been achieved here for the He-like Si, S, and Cl ions. The details of the experiment are presented in this Letter, along with the relativistic [multiconfiguration Dirac-Fock (MCDF)] calculations to evaluate the energies for this transition for the above mentioned ions for the first time. To assess the effect of the relativistic and QED contributions to the energies, we have also made a precise nonrelativistic calculation using a Hylleraas basis set.

The study of this particular transition has been restricted to the helium atom only [18,20]. This is in part due to the fact that, as Z increases along the isoelectronic sequence, the lifetime of the state is reduced, making it difficult to observe it in the laboratory. Also, in comparison with the He atom, the case of He-like heavy ions with higher Z is experimentally more challenging. Hence, the experimental conditions have to be chosen carefully, as described below.

The beams of highly charged Si, S, and Cl ions were obtained from a 14 MV tandem Pelletron accelerator

facility in TIFR Mumbai. The accelerated ion beams selected were not in the He-like charge state to begin with, but were stripped to the He-like charge state. For this purpose, the ions with initially lower charge states were made to pass through a postacceleration carbon stripper foil of thickness $\sim 30\ \mu g/cm^2$. The beam energies used in the experiment were 85 MeV (Cl^{7+}), 84 MeV (S^{7+}), and 80 MeV (Si^{7+}). Under these conditions, it is expected that the charge state distribution will reach an equilibrium value within the target foil. The beam energies and target thickness were chosen so as to ensure not only that the yield of the He-like charge state was sufficient, (i.e., at least about 20%–30%) for the x-ray measurement, but also that the beam energy was sufficient to excite a significant fraction of He-like ions to the doubly excited states.

The x-rays emitted by the projectile ions of different charge states in the foil were measured using a high-resolution bent-crystal x-ray spectrometer [22]. Briefly, this spectrometer consists of a curved ADP (101) crystal mounted in a Johannson geometry, with a Rowland circle diameter of 25.4 cm. The detector is a gas-flow proportional counter, with a continuous circulation of P-10 gas at a pressure slightly greater than 1 atm. The detector was characterized separately using an Am^{241} radioactive source. The entire spectrometer assembly is housed in a stainless steel vacuum chamber. A view port is available to facilitate the proper positioning of the target. The typical vacuum in the chamber is $\sim 2 \times 10^{-6}$ Torr. The resolution was found to be 2.2 eV at Al K_α x-ray energy. The x rays were measured at a backward angle ($\sim 140°$) with respect to the projectile beam direction. Hence, the observed x-ray energies were Doppler shifted to lower energies. This is advantageous to the measurement, as the resolution of the spectrometer is better at lower energies, since $(d\lambda/\lambda) \propto \cot\theta$.

A typical spectrum for the Cl projectile ion is shown in Fig. 1. The first group of lines is predominantly due to Li-like and some He-like transitions. The second group of lines, centered around the H-like Lyman-α line [$2p(^2P^o) \rightarrow 1s(^2S^e)$], contains the transitions of interest in the present study. We focus on this "trio" of lines (see the inset to Fig. 1) consisting of the transitions $2p^2(^3P^e) \rightarrow 1s2p(^3P^o)$, $2p(^2P^o) \rightarrow 1s(^2S^e)$, and $2p3d(^1P^o) \rightarrow 1s3d(^1D^e)$. These lines have been labeled as (A), (B), and (C), respectively. The corresponding transitions are also represented in the diagram in Fig. 2.

Detailed spectra in the region of interest, for all the three ions, are shown in Fig. 3. Panels (a), (b), and (c) show the spectrum for Si, S, and Cl, respectively. The theoretical predictions of line energies are shown as vertical bars. The largest peak in these trios of lines corresponds to the $2p(^2P^e) \rightarrow 1s(^2S^o)$ (Ly-α) transition. The peak on the lower energy side of the Ly-α line corresponds to the $2p^2(^3P^e) \rightarrow 1s2p(^3P^o)$ transition in the He-like ions.

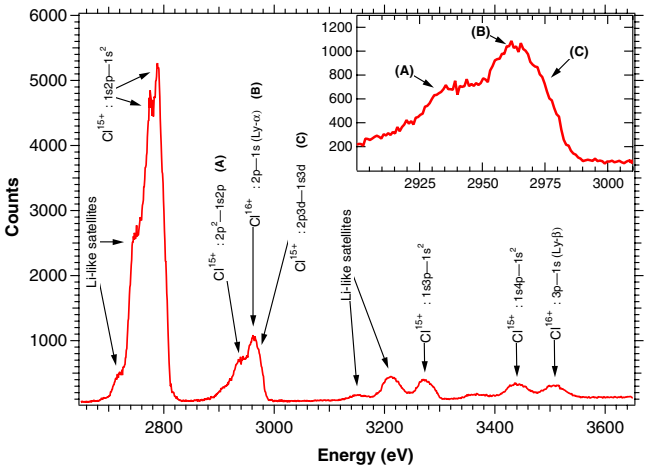

FIG. 1 (color online). Full spectrum from Cl ions, showing Li-like, He-like, and H-like lines. The inset is an expanded view of the region of interest in the present study.

Also, in every case, a slight shoulder is seen on the higher energy side of the Ly-α line. This is most prominent for the Cl projectile ion. Panel (d) of Fig. 3 shows the same data as (c), i.e., for Cl, but the fitting has been carried out with only a single peak near the Ly-α line. As seen in this case, the transition labeled by 'C' as predicted by the theory is not seen and the residuals are also much larger, indicating the need for a better fit. The fitting was carried out using a standard multiparameter least squares fitting algorithm. The same effect is observed in the data for the Si and S ions (not shown in the figure).

The additional line is seen in all the three projectiles, with energy slightly higher than the corresponding H-like Ly-α transition. According to our calculations, this line corresponds to the He-like $2p3d(^1P^o) \rightarrow 1s3d(^1D^e)$ transition. Its proximity to the H-like Ly-α line is probably the major reason for it not being seen in earlier experiments using highly charged ions. There will invariably be some yield of the H-like ions in any method used to collisionally excite the doubly excited He-like states, and the prominent Ly-α transition (which is an allowed $E1$ transition) will swamp the $2p3d(^1P^o) \rightarrow 1s3d(^1D^e)$ transition. The good

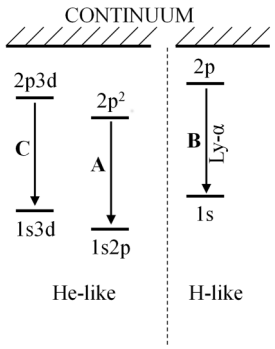

FIG. 2. Diagram of the transitions in the region of interest.

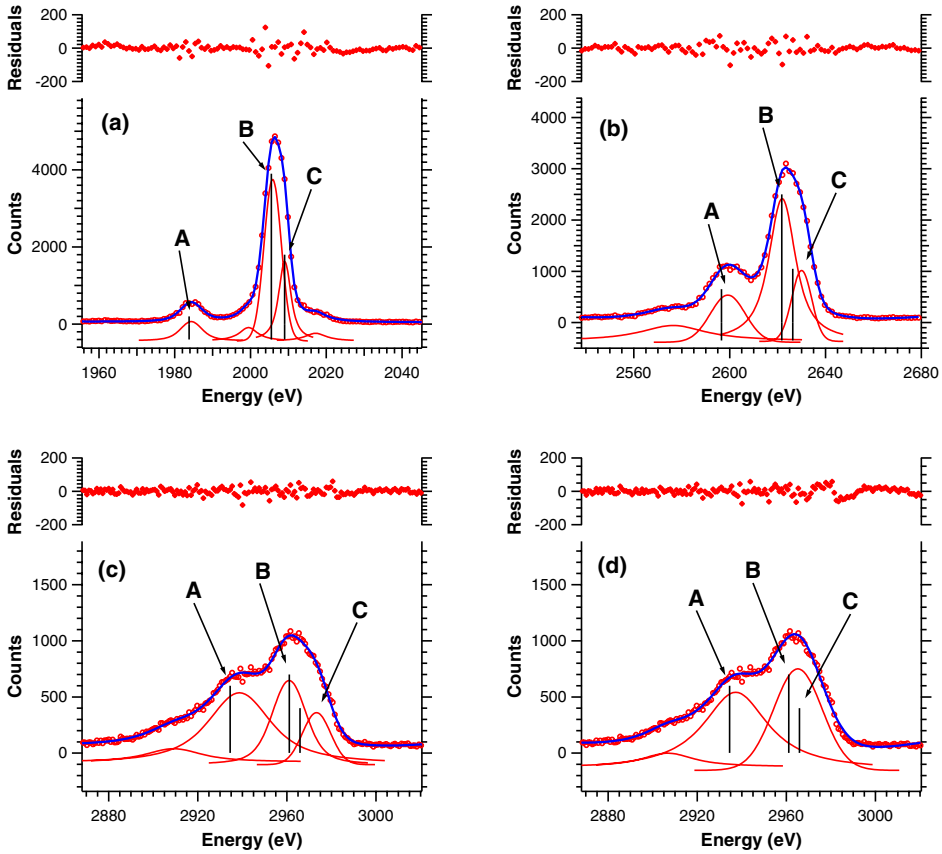

FIG. 3 (color online). Detailed x-ray spectra in the region of interest for (a) Si, (b) S, and (c) Cl ions. The individual peaks are Voigt line shapes fitted to the experimental data. Vertical lines are theoretically predicted line positions. Panel (d) contains the same data as in (c), in which only a single peak is fitted near the position of the Ly-α line, leading to much poorer agreement of the line position, and an increase in the fitting residuals.

resolution of our spectrometer jointly with relatively higher fraction of He-like ions in the foil enables us to just resolve these two very nearby lines. To exclude other possibilities, we have calculated the line energies for similar transitions, such as the $2p4d(^1P^o) \rightarrow 1s4d(^1D^e)$ transition, and the obtained values are 2006.84, 2623.52, and 2963.00 eV for the Si^{12+}, S^{14+}, and Cl^{15+} ions, respectively. Clearly they differ from the measured $2p3d(^1P^o) \rightarrow 1s3d(^1D^e)$ lines by more than the experimental uncertainties. In fact, the $2p4d(^1P^o) \rightarrow 1s4d(^1D^e)$ line in each case approaches and is very close (within about 1.3–3.2 eV) to the Ly-α line for which the line energies are 2005.5, 2621.7, 2959.8 eV, for He-like Si, S, and Cl, respectively. The question of such fluorescence transitions for triplet states in the present experiment does not arise at all, because for the triplet states the autoionization probability is larger than that for fluorescence. For example, even for helium, the autoionization rate of the $2p3d(^3P^o)$ state is 18.8×10^9 s^{-1} compared to the fluorescence rate of 6.58×10^9 s^{-1} [15].

Accurate experimental determination of such transitions goes side by side with precise theoretical calculations which include several relativistic and QED effects. We have made both relativistic and nonrelativistic calculations for the transition energies in the different charge states of different projectile ions. The relativistic calculations were made within the MCDF approach using the state-of-the-art general relativistic MCDF code (MDFGME) developed by Desclaux and Indelicato [23,24]. To compute the wave function and energy for each state involved in a transition, the so-called optimized level method was followed. Consequently, the spin orbitals in the initial and final states for the radiative transitions are not orthogonal, since they have been optimized separately. Radiative corrections, such as the one-electron self-energy, the self-energy screening, and vacuum polarization were also included, from a full QED treatment. The description of the code as well as the method is given in Refs. [25,26].

We have chosen the multiconfiguration approach because this method enables the inclusion of a large amount of electronic correlation by taking into account a small number of configurations. In a preliminary calculation, all transition energies and probabilities were computed in a monoconfiguration approach. Afterwards, we used a virtual space spanned by single- and double-excited configurations, up to the $4f$ subshell.

To emphasize the importance of relativistic and QED effects as well as to assess the extent of the corresponding corrections, we have also compared our results with extremely accurate nonrelativistic calculations. This calculation uses an explicitly correlated wave function in a Hylleraas basis set, in the framework of the stabilization method [27]. A portion of the stabilization diagram using a 450 parameter Hyleraas basis set for $^1P^o$ states of Cl^{15+} is given in Fig. 4(a). In this figure, as an example, we have plotted the 15th to the 30th eigenroots in the energy range -80.0 a.u. to -40.0 a.u. It is evident from Fig. 4(a) that each energy eigenroot changes with the soft wall [27] of the basis and there exists a flat plateau in the vicinity of avoided crossings for some particular energy value. This confirms the presence of resonance states in the neighborhood of that energy value. The fourth $^1P^o$ resonance state originating from the $2p3d$ configuration of Cl^{15+} exists near about -50.0 a.u. as is evident from Fig. 4(a). The density of states is estimated by evaluating the inverse of the slope at several points near the flat plateau region of each energy eigenroot and fitting to a standard Lorentzian profile, yielding the position E_r and width Γ of the resonance state.

Among different fitting curves for each energy eigenroot corresponding to a particular resonance state, the fitting curve with the least square sum (χ^2) and the square of correlation (R^2) closer to unity leads to the desired resonance energy E_r and width Γ. The density of resonance states and the corresponding fitted Lorentzian ($\chi^2 = 0.006\,796$, $R^2 = 0.999\,94$), illustrated in Fig. 4(b), yields the resonance position at -50.117 a.u. (-1363.75 eV) and a width of 1.0523×10^{-4} a.u. (4.35×10^{12} s^{-1}) for the $2p3d(^1P^o)$ state of the Cl^{15+} ion. The above mentioned fitting parameters (χ^2, R^2) can be compared to the values of (0.007 497, 0.999 59) and (0.012 904, 0.997 54) for two other fitted Lorentzian curves, respectively. The same procedure was carried out for each ion under study.

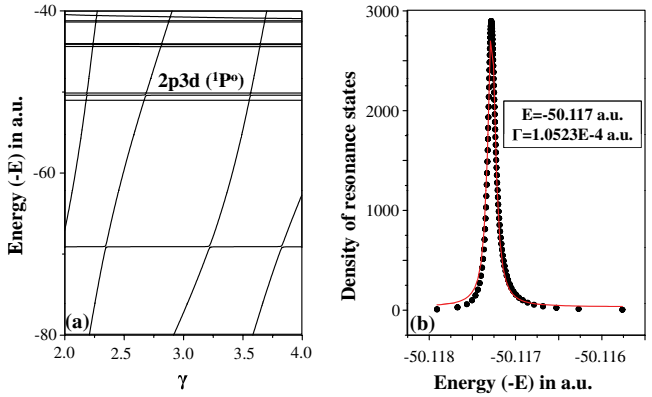

FIG. 4 (color online). (a) Stabilization diagram for $^1P^o$ states of Cl^{15+}. (b) Calculated density (circles) and the fitted Lorentzian (solid line) for the $2p3d(^1P^o)$ resonance state of Cl^{15+} [21st root].

All calculations were made in quadruple precision to ensure numerical stability [27].

A comparison of the experimental line energy for the $2p3d(^1P^o) \rightarrow 1s3d(^1D^e)$ transition, as well as the line positions calculated with the MDFGME code, is shown in Table I. Also shown are the nonrelativistic calculations, which differ from the relativistic calculations by a few to several electron volts in every case. To be precise, the contributions of the relativistic and QED effects are the largest (11 eV for Si^{12+} to 26 eV for Cl^{15+}) in the ground state [$1s^2(^1S^e)$] energy. This decreases for the singly excited [$1s2p(^3P^o)$ and $1s3d(^1D^e)$] states: 7 eV for Si^{12+} to 17 eV for Cl^{15+}, and 6 eV for Si^{12+} to 14 eV for Cl^{15+}, respectively. For the doubly excited states $2p^2(^3P^e)$ and $2p3d(^1P^o)$, the differences are further reduced: 1 eV for Si^{12+} to 4 eV for Cl^{15+}, and 2 eV for Si^{12+} to 5 eV for Cl^{15+}, respectively.

In estimating the uncertainty in the experimental values for the $2p3d(^1P^o) \rightarrow 1s3d(^1D^e)$ line energy, we have taken into account the uncertainties in fitting and calibration. For example, for Si, the respective contributions of these two sources are $\pm 0.01\%$ (0.2 eV) and $\pm 0.05\%$ (1.0 eV), which when combined additively give an overall uncertainty of $\pm 0.06\%$ (1.2 eV). Similarly, the overall uncertainties in S an Cl are $\pm 0.13\%$ (3.5 eV) and $\pm 0.29\%$ (8.7 eV), respectively. The increasing uncertainties can be attributed to the poorer resolution of the spectrometer with increasing energy. In all three cases, the line energies seem to be slightly larger than the theoretical predictions. While the values lie within the experimental uncertainties for Si and Cl, in the case of S, the difference is only a little (~ 0.2 eV) beyond the uncertainty. Hence, the overall agreement between experiment and theory is seen to be excellent.

To the best of our knowledge, this is the first accurate experimental determination of the radiative decay of this $2p3d(^1P^o)$ state for highly charged ions, since many earlier studies probably have neglected it as being an autoionizing state according to the standard selection rules. Also, the proximity of this line to the H-like Ly-α line makes it observable only with high resolution spectroscopy. Our experimental results show a clear evidence of the enhanced stability of the $2p3d(^1P^o)$ state against

TABLE I. Measured line energies, and those predicted from the relativistic as well as nonrelativistic calculations for the $2p3d(^1P^o) \rightarrow 1s3d(^1D^e)$ transition. The last column gives the difference between the experiment and the relativistic theory.

	Transition energy E(eV)			ΔE
	Theory			$E_{\text{Expt.}} - E_{\text{Rel}}$
Ion	NR	Rel	Expt.	(eV)
Si^{12+}	2005.04	2009.00	2009.0 ± 1.2	+0.0
S^{14+}	2618.09	2626.32	2630.0 ± 3.5	+3.7
Cl^{15+}	2955.24	2965.93	2973.0 ± 8.7	+7.1

TABLE II. Fluorescence (Γ_f) and autoionization (Γ_a) rates for the $2p3d(^1P^o)$ state in Si^{12+}, S^{14+}, and Cl^{15+}, as well as the respective fluorescence yields (f). Also shown for comparison are the corresponding values for He.

Ion	Γ_f (s^{-1})	Γ_a (s^{-1})	f (%)
Si^{12+}	3.280×10^{13}	3.204×10^{12}	91.10
S^{14+}	2.735×10^{13}	3.901×10^{12}	87.52
Cl^{15+}	3.012×10^{13}	4.350×10^{12}	87.38
He	5.11×10^{9}	1.38×10^{8}	97.37

autoionization, which is in accord with the criterion prescribed by Saha *et al.* [21].

To substantiate this argument quantitatively, we have also calculated the fluorescence rate for the $2p3d(^1P^o)$ state of Cl^{15+}, S^{14+}, and Si^{12+} by extending the methodology used by Saha *et al.* [21]. The results obtained are shown in Table II. It is interesting to note that, although the autoionization rate for the $2p3d(^1P^o)$ state for these highly charged ions ($\sim 10^{12}$ s^{-1}) is substantially increased compared to that for helium ($\sim 10^{8}$ s^{-1}), the fluorescence rate also grows with Z in such a way that the radiative decay channel can compete with the autoionization channel. The above reason makes it possible to observe the spectral line corresponding to the transition $2p3d(^1P^o) \rightarrow 1s3d(^1D^e)$ with sufficient yields.

The authors would like to acknowledge the Pelletron accelerator staff for the smooth running of the machine during the experiment, and N. Mhatre for technical assistance. J. P. S. and A. M. C. acknowledge the support by FCT–Fundação para a Ciência e a Tecnologia (Portugal), through Projects No. PEstOE/FIS/UI0303/2011 and No. PTDC/FIS/117606/2010. Laboratoire Kastler Brossel is UMR No. 8552 of the ENS, CNRS, and UPMC. T. K. M. and J. K. S. are thankful to the Department of Atomic Energy, BRNS, Government of India, for financial assistance under Grant No. 2011/37P/15/BRNS/0074.

*lokesh@tifr.res.in

[1] R. P. Madden and K. Codling, Phys. Rev. Lett. **10**, 516 (1963).
[2] J. W. Cooper, U. Fano, and F. Prats, Phys. Rev. Lett. **10**, 518 (1963).
[3] A. K. Bhatia and A. Temkin, Rev. Mod. Phys. **36**, 1050 (1964).
[4] H. G. Berry, Phys. Scr. **12**, 5 (1975).
[5] C. D. Lin, Phys. Scr. **T46**, 65 (1993).
[6] M. Domke, K. Schulz, G. Remmers, G. Kaindl, and D. Wintgen, Phys. Rev. A **53**, 1424 (1996).
[7] G. Tanner, K. Richter, and J.-M. Rost, Rev. Mod. Phys. **72**, 497 (2000).
[8] E. U. Condon and G. H. Shortley, *The Theory of Atomic Spectra* (Cambridge University Press, Cambridge, England, 1935).
[9] P. Feldman and R. Novick, Phys. Rev. Lett. **11**, 278 (1963).
[10] A. B. C. Walker, Jr. and H. R. Rugge, Astrophys. J. **164**, 181 (1971).
[11] A. H. Gabriel and C. Jordan, Mon. Not. R. Astron. Soc. **145**, 241 (1969).
[12] T. Fujimoto and T. Kato, Astrophys. J. **246**, 994 (1981).
[13] T. W. Gorczyca, J.-E. Rubensson, C. Såthe, M. Ström, M. Agåker, D. Ding, S. Stranges, R. Richter, and M. Alagia, Phys. Rev. Lett. **85**, 1202 (2000).
[14] C.-N. Liu, M.-K. Chen, and C. D. Lin, Phys. Rev. A **64**, 010501 (2001).
[15] M. Žitnik, K. Bučar, M. Štuhec , F. Penent, R. I. Hall, and P. Lablanquie, Phys. Rev. A **65**, 032520 (2002).
[16] J.-E. Rubensson, C. Såthe, S. Cramm, B. Kessler, S. Stranges, R. Richter, M. Alagia, and M. Coreno, Phys. Rev. Lett. **83**, 947 (1999).
[17] M. K. Odling-Smee, E. Sokell, P. Hammond, and M. A. MacDonald, Phys. Rev. Lett. **84**, 2598 (2000).
[18] J. G. Lambourne, F. Penent, P. Lablanquie, R. I. Hall, M. Ahmad, M. Žitnik, K. Bučar, M. K. Odling-Smee, J. R. Harries, P. Hammond, D. K. Waterhouse, S. Stranges, R. Richter, M. Alagia, M. Coreno, and M. Ferianis, Phys. Rev. Lett. **90**, 153004 (2003).
[19] M. Coreno, M. de Simone, M. Danailov, R. Richter, A. Kivimki, M. Zitnik, and K. Prince, J. Electron Spectrosc. Relat. Phenom. **144–147**, 39 (2005).
[20] M. Coreno, K. C. Prince, R. Richter, M. de Simone, K. Bučar, and M. Žitnik, Phys. Rev. A **72**, 052512 (2005).
[21] J. Saha, S. Bhattacharyya, P. Mukherjee, and T. Mukherjee, Chem. Phys. Lett. **517**, 223 (2011).
[22] A. Kumar, D. Misra, K. Thulasiram, L. Tribedi, and A. Pradhan, Nucl. Instrum. Methods Phys. Res., Sect. B **248**, 247 (2006).
[23] J. P. Desclaux, Comput. Phys. Commun. **9**, 31 (1975).
[24] P. Indelicato and J. P. Desclaux, Phys. Rev. A **42**, 5139 (1990).
[25] P. Indelicato, Phys. Rev. Lett. **77**, 3323 (1996).
[26] J. P. Santos, G. C. Rodrigues, J. P. Marques, F. Parente, J. P. Desclaux, and P. Indelicato, Eur. Phys. J. D **37**, 201 (2006).
[27] J. K. Saha and T. K. Mukherjee, Phys. Rev. A **80**, 022513 (2009).